On-Shaft Wireless Vibration Measurement Unit and Signal Processing Method for Torsional and Lateral Vibration

Ivar Koene, Sampo Haikonen, Tuomas Tiainen, Joni Keski-Rahkonen, Mikael Manngård, *Graduate Student Member, IEEE*, and Raine Viitala

***Abstract*—Microelectromechanical systems accelerometers have opened new possibilities for vibration monitoring of a rotating machinery. They enable mounting accelerometers directly to the rotating component of the machine, e.g., shaft. This enables not only the measurement of a lateral vibration but also a torsional vibration of the machine. This increases the vibration data gathered from the machine by one measurement instrument. This article presents an on-shaft wireless universal measurement unit (UMU) with innovative combination of features, such as a high measurement range and easy mounting. The UMU has a two-sensor configuration where two accelerometers are mounted to the opposite sides of a shaft. This enables to utilize a novel signal processing method to separate torsional and lateral vibration from the data. The signal processing method combines and modifies methods presented in the published literature. The results presented in this article demonstrate that the UMU together with the presented signal processing method can measure frequencies of torsional and lateral vibration accurately. However, the amplitude comparison between the UMU and reference sensors cannot be done adequately because they are measuring either different components of the machine or different physical properties.**

***Index Terms*—Accelerometer, condition monitoring, lateral vibration, microelectromechanical systems (MEMS), torsional vibration.**

Manuscript received 7 February 2022; revised 7 May 2022; accepted 19 June 2022. Date of publication 27 July 2022; date of current version 14 December 2022. Recommended by Technical Editor Z. Zhu and Senior Editor H. Gao. This work was supported in part by the Business Finland Reboot IoT Factory under Grant 4356/31/2019 and in part by the Academy of Finland under Grant AI-ROT, 335717. *(Corresponding author: Ivar Koene.)*

Ivar Koene, Sampo Haikonen, Tuomas Tiainen, and Raine Viitala are with the School of Engineering, Aalto University, 02150 Espoo, Finland (e-mail: ivar.koene@aalto.fi; sampo.haikonen@aalto.fi; tuomas.tiainen@aalto.fi; raine.viitala@aalto.fi).

Joni Keski-Rahkonen is with Kongsberg Maritime Finland Oy, 26100 Rauma, Finland (e-mail: joni.keski-rahkonen@km.kongsberg.com).

Mikael Manngrd is with the Faculty of Science and Engineering, Åbo Akademi University, 20500 Turku, Finland (e-mail: mikael.manngard@abo.fi).

Color versions of one or more figures in this article are available at https://doi.org/10.1109/TMECH.2022.3189954.

Digital Object Identifier 10.1109/TMECH.2022.3189954

I. Introduction

A TYPICAL method to perform measurements of rotating machinery for condition-monitoring purposes is to mount accelerometers to a static part of the machine, e.g., a bearing housing or frame. Mounting accelerometers to static parts of the machine enables the measurement of lateral vibration, which can provide information of wear or damage in bearings and gears and detect unbalance in rotating components. However, in many applications, such as powertrains, it is also important to gain data about torsional loads and their induced vibration. The measurement of torsional vibration is key for understanding the true loads acting in the driveline. This information can be utilized for research and development purposes, for the design of driveline components against measured and known load profiles, and for root cause analysis of vibration problems.

Often, sensors, which measure torsional vibration need to be mounted to the rotating part of the machine. Hence, the data acquisition and measurement setup are more challenging compared to the sensors mounted to static parts. The two most common ways of measuring torsional vibration are pulse sensors [1]–[3], which measure angle or velocity, and strain gauges [4]–[6], which measure the deformation of a component.

Accelerometers can also be used to measure torsional vibration by mounting them directly to the shaft. However, on-shaft accelerometers will measure both lateral and torsional vibration as well as gravitational acceleration. The separation of the torsional and lateral vibration and removal of gravitational component can be achieved with a specific sensor configuration and signal processing methods [7], [8].

Lin and Kuang [7] studied the sensor configuration and signal processing method to separate the torsional and lateral vibration from on-shaft accelerometer data. They used a symmetric sensor configuration in which two accelerometers were mounted to the opposite sides of the shaft. They separated the lateral or torsional vibration from the data by subtracting or adding the accelerometer signals.

The rotation movement of the on-shaft accelerometers causes gravitational force to produce a sinusoidal signal to the acceleration data with a frequency equal to the rotational speed and 1 g amplitude. Typically, this gravity component needs to be eliminated to examine the rest of the data properly. On this point, Mones et al. [8] studied two different methods to remove

gravity from the signal. The first method included only one accelerometer with two measurement axes: one for tangential acceleration and one for radial acceleration. The removal of the gravity component from the tangential acceleration data starts by phase shifting the radial signal by 90° with the Hilbert transform. The shifted signal is added to the tangential signal, which removes the gravity component from the signal. Another method for removing gravity from measurement data, as presented by Mones et al. [8], is to mount two sensors to the opposite sides of the shaft and calculate the mean value from the data in similar manner to Lin and Kuang [7]. This will remove the lateral vibration as well as the gravity component. The first aforementioned method will only remove the gravity component but not the lateral vibration.

Elnady [9] and Koene et al. [10] studied a method exploiting rotation matrix to separate horizontal and vertical lateral vibration from a measurement of on-shaft accelerometer. However, both studies only used one two-axes accelerometer. Elnady [9] mounted the accelerometer on the surface of the shaft and Koene et al. [10] aligned the sensor with the central axis of the shaft. Elnady's method disabled the possibility to decompose torsional and lateral vibration from the measurement data. In addition, Elnady was required to use high-pass and stop-band filtering to remove a constant acceleration from the radial acceleration and remove gravity component from both radial and tangential acceleration signals. The filtering could remove important information from the data as Elnady also stated in his study. The sensor mounting of [10] enabled to measure only the lateral vibration, thus, they did not need to remove torsional vibration form the data. However, aligning the accelerometer with the central axis of the shaft can be challenging or in some cases even impossible, which limits its applications.

On-shaft accelerometers have been studied with piezoelectric [7] and microelectromechanical systems (MEMS) accelerometers [8]–[15]. Piezoelectric accelerometers typically have wired data transfer, which makes the data acquisition more challenging when the sensor is rotating with the shaft. In contrast, compact and low-powered MEMS accelerometers allow to use battery as a power source and wireless data transfer, which make them convenient in on-shaft sensor applications.

Several studies have been conducted where on-shaft accelerometers have been used to measure lateral [9]–[11], [13] or torsional vibration [12], [14], [15]. However, in many of these studies, only one accelerometer is mounted on the shaft [9], [11], [14], [15], and they have not taken into consideration that both lateral and torsional vibration are measured with that sensor configuration. Nevertheless, they were able to achieve good results because in their applications the separation of lateral and torsional vibration was not necessary. In applications where the torsional and lateral vibration need to be investigated separately, these methods might not be applicable. For example, with a ship propulsion, it is important to know the torsional loads, which can be determine from torsional vibration. On the other hand, the lateral vibration can be used to monitor condition of components, such as bearings. Thus, it is important to monitor both vibrations separately in some applications.

We report a contribution beyond the state-of-the-art as follows.

1) A new design and realization of a wireless on-shaft universal measurement unit (UMU) for vibration measurement.
2) The UMU combines high sampling rate (up to 20 kHz), high sensitivity (20 mV/g), high measurement range (±40 g), high bandwidth (2.4 kHz), and fast and easy mounting to a shaft with free surface area.
3) A new signal processing method to decompose different vibration signals from data of the UMU, which combines and modifies the algorithms presented in [7], [9], and [10] to work with symmetric sensor configuration.

The UMU is battery powered and has wireless communication over wireless local area network (WLAN), which allowed for easy mounting and operation. Moreover, two two-axes accelerometers were mounted to the opposite sides of the shafts, measuring radial, and tangential accelerations. The UMU was designed and optimized for on-shaft measurement applications.

The novel signal processing method advances the previously presented research on the on-shaft accelerometer signal processing methods. By combining and modifying the algorithms presented in [7], [9], and [10] to work the with symmetric two-sensor configuration, the method proposed by this article enables one to extract torsional and lateral vibration signals from the rotating on-shaft accelerometer data. Moreover, the lateral vibration signal is decomposed into its horizontal and vertical vibration components. This complete decomposition of the on-shaft accelerometer data is developed and presented in this article integrally for the first time. With the presented method, no filtering is required to decompose the signal, thus, less information is lost during the signal processing. The UMU and signal processing method was verified with measurements of torsional and lateral vibration with typical commercially available sensors. In this article, the torsional vibration is observed with measurements of tangential and radial acceleration (UMU) and torque fluctuation (reference torque transducer).

The rest of this article is organized as follows. Section II describes the UMU, signal processing and test environment, Sections III and IV present the results and discussion, and finally, Section V concludes this article.

II. Universal Measurement Unit and Signal Processing

The UMU presented in this article is based on an Internet of things vibration measurement device called Memsio, which was published by Koene et al. [16]. This article extends the previous research by presenting a modification of the setup for a new application. In particular, the on-shaft measurement required a second accelerometer, higher range accelerometers, and upgraded data acquisition with an analog-to-digital converter (ADC). In addition, the housing needed to be designed for the on-shaft mounting.

A. Components and Sensor Configuration

The UMU consists of a microcontroller (ESP32-WROVER) with Internet connection capabilities (see [16]), SD-card, 750

TABLE I
SPECIFICATIONS OF ADXL356C (ANALOG DEVICES)

Measurement range (g)	±10, ±40
Sensitivity (mV/g)	80, 20
Noise density (μ*Hz$^{-1/2}$)	75, 110
Bandwidth (kHz)	2.4

TABLE II
SPECIFICATIONS OF AD7689 (ANALOG DEVICES)

Max. voltage range (V)	5
Resolution (bit)	16
Bandwidth (kHz)	250
Channels	8

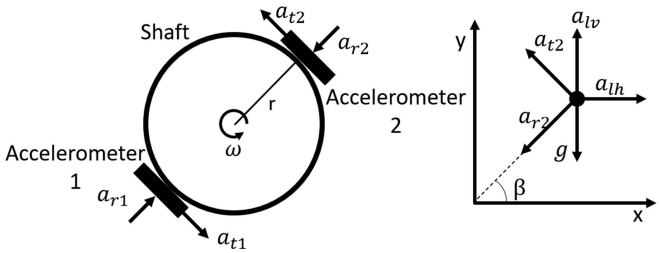

Fig. 1. Sensor configuration of the UMU. The a_{r1} and a_{r2} are the radial measurement axes, and a_{t1} and a_{t2} are the tangential measurement axes of the accelerometers. r is the distance of the sensors from the shaft central axis, and it is approximately 7.5 mm. The right-hand side of the picture presents a free body diagram of one of the accelerometers. a_{r2} is the radial acceleration of accelerometer 2, a_{2t} is the tangential acceleration of accelerometer 2, g is the gravitational acceleration, a_{lv} is the lateral vertical vibration, and a_{lh} is the lateral horizontal vibration.

mAh lithium-ion battery, ADC (AD7689), hall sensor (SS441R), and two MEMS accelerometers (ADXL356C). The specifications of the accelerometer and ADC can be found in Tables I and II, respectively.

The accelerometer configuration can be seen in Fig. 1. The ADXL356 accelerometers are placed on the opposite sides of the shafts. Both sensors measure two directions: radial and tangential. The UMU and the sensors are mounted to the shaft with a 3D-printed housing made from polylactide. The accelerometers and hall sensor have a separate housing from the other components to allow for more accurate mounting to the shaft. The UMU is presented in Fig. 2.

B. Data Acquisition

The UMU is controlled via a browser-based graphical user interface (GUI), which is similar to the Memsio GUI [16]. From the GUI, the sampling rate and measurement time can be selected, and measurement data downloaded. The GUI makes the measurement process effortless because the UMU can be operated with any device that has an Internet connection and a browser; no extra software is needed.

The microcontroller conducts the data acquisition. At the beginning of the measurement, the microcontroller disconnects itself from the Internet and shuts down the WLAN. This is done to maximize the processing power to the data acquisition during

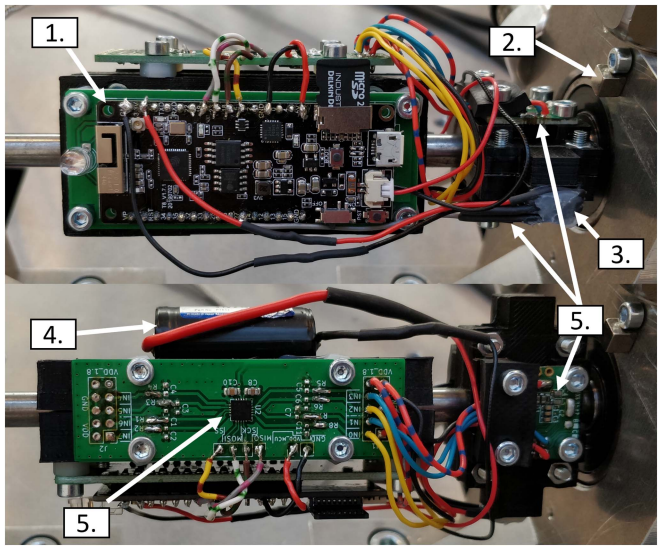

Fig. 2. UMU mounted to the shaft. (1) Microcontroller. (2) Magnet for the hall sensor. (3) Hall sensor. (4) Battery. (5) Accelerometers. (6) Analog to digital converter.

the measurement. The measurement time is predetermined using the GUI. When the measurement is finished, the UMU turns on the WLAN and connects back to the Internet. The data are stored to an SD card during the measurement with the help of a circular buffer. The measurement data can be downloaded after the measurement using the GUI. The data acquisition allows a maximum of 20 kHz sampling rate without any significant jitter. The accelerometers had fixed low pass filters with a cutoff frequency of 2.4 kHz. A magnet was mounted to the bearing housing next to the UMU to obtain a once per rotation pulse from the hall sensor.

C. Signal Processing

The signal processing was completed with MATLAB software.

1) Calibration: After mounting the UMU to the shaft, the accelerometers were calibrated with the help of gravity. The shaft was rotated with a low velocity of 5 r/min; hence, it can be assumed that the only significant acceleration affecting the sensors was gravity. In total, 20 revolutions were measured, and the data were averaged to one revolution for each measurement axes using the hall sensor to inform when the revolution begins and ends. Because the sampling was conducted with a time-based sample clock, there were small changes in the sample count per rotation. This was corrected with a discrete Fourier transform (DFT). The data were converted into the frequency domain, and the few highest frequency components were deleted from the data to obtain the same sample count as with the revolution with the lowest samples per rotation. Next, the frequency domain signal was converted back to the time domain with an inverse DFT. This process made the sample count equal for each revolution without deleting any meaningful data. After the one average round was calculated, the following steps were taken to calculate the correct gains for the binary data.

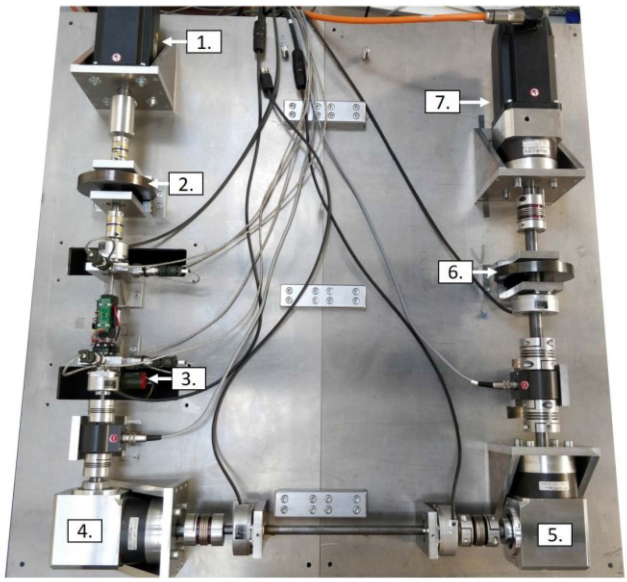

Fig. 3. Small-scale maritime powertrain test bench. (1) Driving motor. (2), (6) Masses to lower the torsional natural frequencies of the powertrain. (3) Lateral sinusoidal excitation device. (4) First gear (1:3). (5) Second gear (1:4). (7) Excitation motor and 8:1 gear.

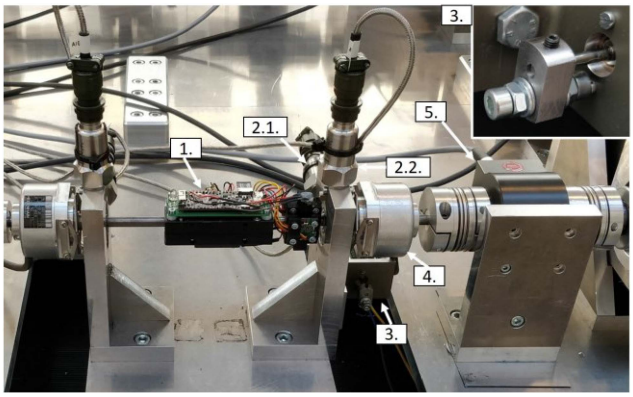

Fig. 4. UMU, reference sensors, and lateral sinusoidal excitation device mounted to the shaft. (1) UMU. (2.1) Accelerometer on bearing housing to measure horizontal lateral vibration. (2.2) Accelerometer on bearing housing to measure vertical lateral vibration. (3) Lateral sinusoidal excitation device. (4) Optical encoder. (5) Torque transducer. Top right corner has a close-up of the unbalance of the lateral sinusoidal excitation device.

1) Calculate the mean value a_{mean} of that average round, which is equal to the zero acceleration value.
2) Calculate the gain to transfer the raw ADC data into m/s2 with the following equation:

$$a_{\text{gain}} = \frac{(\max(a_{\text{ADC}}) - \min(a_{\text{ADC}}))}{2 \cdot 9.81 \frac{m}{s^2}} \tag{1}$$

where a_{ADC} is the raw integer value from the ADC.
3) Equation (2) calculates the m/s2 value for the ADC output of the accelerometers

$$a\ (n) = \frac{a_{\text{ADC}}(n) - a_{\text{mean}}}{a_{\text{gain}}} \tag{2}$$

where n is the sample number.

2) Separation of Lateral and Torsional Vibration: Before presenting the method to separate the torsional and lateral vibration from the data of the UMU, a simple mathematical presentation of the tangential and radial measurements of the MEMS sensors will be presented. The mathematical equations are made based on the free body diagram in Fig. 1. The tangential axes a_{t1} and a_{t2} will measure the tangential acceleration component a_t (3), the gravitational acceleration in tangential direction g_t (4), and lateral acceleration in tangential direction a_{lt} (5). The number indexes 1 and 2 in the tangential axes a_{t1} and a_{t2} indicates the sensors 1 and 2 in Fig. 1

$$a_t = r \cdot \alpha \tag{3}$$

$$g_t = g \cdot \cos(\beta) \tag{4}$$

$$a_{lt} = a_{lh} \cdot \sin(\beta) - a_{lv} \cdot \cos(\beta) \tag{5}$$

where r is the radius marked in Fig. 1, α is the angular acceleration, g is the gravitational acceleration (9.81 m/s^2), a_{lh} is the lateral horizontal acceleration, a_{lv} is the lateral vertical acceleration, and β is the rotational angle of the shaft in the world coordinate system.

The radial axes a_{r1} and a_{r2} of the UMU will consist of radial acceleration component a_r (6), as well as the gravitational component in radial direction g_r (7), and lateral acceleration in radial direction a_{lr} (8). The number indexes 1 and 2 in the radial axes indicates the sensors 1 and 2 in Fig. 1

$$a_r = \omega^2 \cdot r \tag{6}$$

$$g_r = g \cdot \sin(\beta) \tag{7}$$

$$a_{lr} = a_{lh} \cdot \cos(\beta) + a_{lv} \cdot \sin(\beta) \tag{8}$$

where r is the radius marked in Fig. 1, ω is the angular velocity, g is the gravitational acceleration (9.81 m/s^2), a_{lh} is the lateral horizontal acceleration, a_{lv} is the lateral vertical acceleration, and β is the angle of the shaft in the world coordinate system.

The full equations of the two accelerometers in the UMU are presented in (9) and (11). Equations (10) and (12) are received by substituting from (3) to (8) to (9) and (11) as follows:

$$\begin{cases} a_{t1} = a_t + g_t + a_{lt} \\ a_{r1} = a_r - g_r + a_{lr} \end{cases} \tag{9}$$

$$\begin{cases} a_{t1} = r \cdot \alpha + g \cdot \cos(\beta) + a_{lh} \cdot \sin(\beta) - a_{lv} \cdot \cos(\beta) \\ a_{r1} = \omega^2 \cdot r - g \cdot \sin(\beta) + a_{lh} \cdot \cos(\beta) + a_{lv} \cdot \sin(\beta) \end{cases} \tag{10}$$

$$\begin{cases} a_{t2} = a_t - g_t - a_{lt} \\ a_{r2} = a_r + g_r - a_{lr} \end{cases} \tag{11}$$

$$\begin{cases} a_{t2} = r \cdot \alpha - g \cdot \cos(\beta) - a_{lh} \cdot \sin(\beta) + a_{lv} \cdot \cos(\beta) \\ a_{r2} = \omega^2 \cdot r + g \cdot \sin(\beta) - a_{lh} \cdot \cos(\beta) - a_{lv} \cdot \sin(\beta) \end{cases} \tag{12}$$

Separation of the lateral and torsional vibration was completed similarly as Lin and Kuang [7] outlined in his article. Equation (13) presents the torsional tangential acceleration, which is calculate using the a_{t1} and a_{t2}. After tangential accelerations from (10) and (12) are substituted to (13), the removal of gravitational component and lateral vibration can be observed

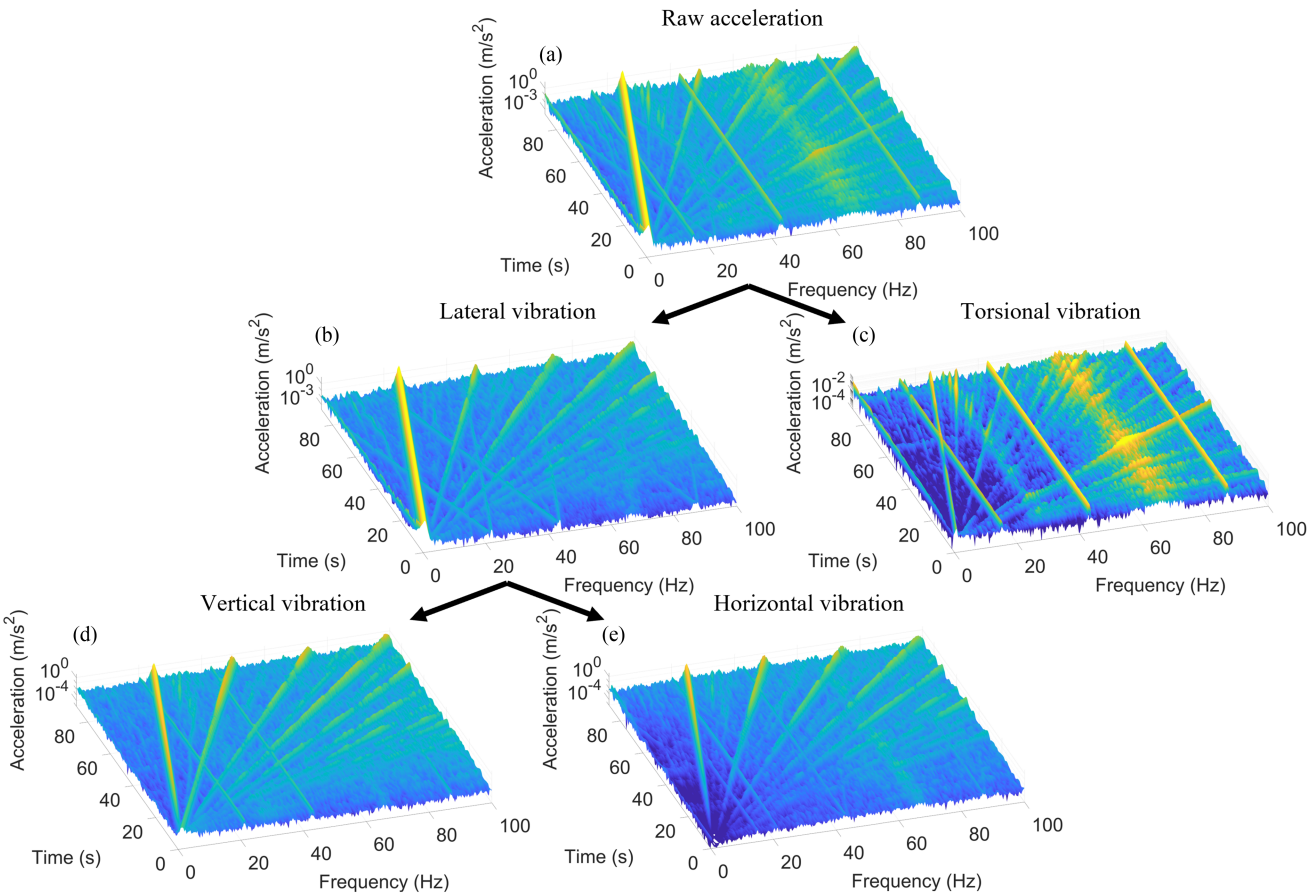

Fig. 5. Separation of the vibration data from the raw accelerometer data measured with the UMU presented as STFT plots. (a) Raw acceleration data from $\boldsymbol{a_{t2}}$. (b) Lateral vibration calculated from tangential acceleration data (17). (c) Torsional vibration calculated from tangential acceleration data (13). (d) Vertical lateral vibration. (e) Horizontal lateral vibration calculated with (22).

in (14) and only the tangential acceleration component is left

$$a_{tt} = \frac{a_{t1} + a_{t2}}{2} \tag{13}$$

$$a_{tt} = r \cdot \alpha. \tag{14}$$

Equation (15) presents the torsional radial acceleration, which is calculate by using the radial accelerations a_{r1} and a_{r2}. When radial accelerations from (10) and (12) are substituted to (15), the same gravity and lateral vibration removal can be observed is in (14) and only the radial acceleration component is left as seen in (16) as follows:

$$a_{tr} = \frac{a_{r1} + a_{r2}}{2} \tag{15}$$

$$a_{tr} = \omega^2 \cdot r. \tag{16}$$

The lateral vibration from the tangential and radial accelerations are calculated with (17) and (19), respectively. When the accelerations from (10) and (12) are substituted to the equations, the tangential and radial accelerations are removed but the gravitational component and lateral vibration are still present, which can be seen in (18) and (20) as follows:

$$a_{lt} = \frac{a_{t1} - a_{t2}}{2} \tag{17}$$

$$a_{lt} = g \cdot \cos(\beta) + a_{lh} \cdot \sin(\beta) - a_{lv} \cdot \cos(\beta) \tag{18}$$

$$a_{lr} = \frac{a_{r1} - a_{r2}}{2} \tag{19}$$

$$a_{lr} = -g \cdot \sin(\beta) + a_{lh} \cdot \cos(\beta) + a_{lv} \cdot \sin(\beta). \tag{20}$$

Equations (13) and (15) remove the gravitational component from the data. However, in the lateral vibration, the gravitational acceleration is still present, and the direction of the vibration is unknown. To remove the gravity component and decompose the vertical and horizontal vibration, the following method was used.

1) Calculate the moving average from both lateral vibration signals (a_{lt} and a_{lr}) to remove the high frequency components.
2) Utilize (21) to calculate the phase of the shaft based on the positions of the accelerometers

$$\beta = \tan^{-1}\left(\frac{a_{lt_{ma}}}{a_{lr_{ma}}}\right) \tag{21}$$

where $a_{lt_{ma}}$ is the moving average of the lateral vibration calculated from the tangential accelerations and $a_{lr_{ma}}$ is the moving average of the lateral vibration calculated from the radial acceleration.

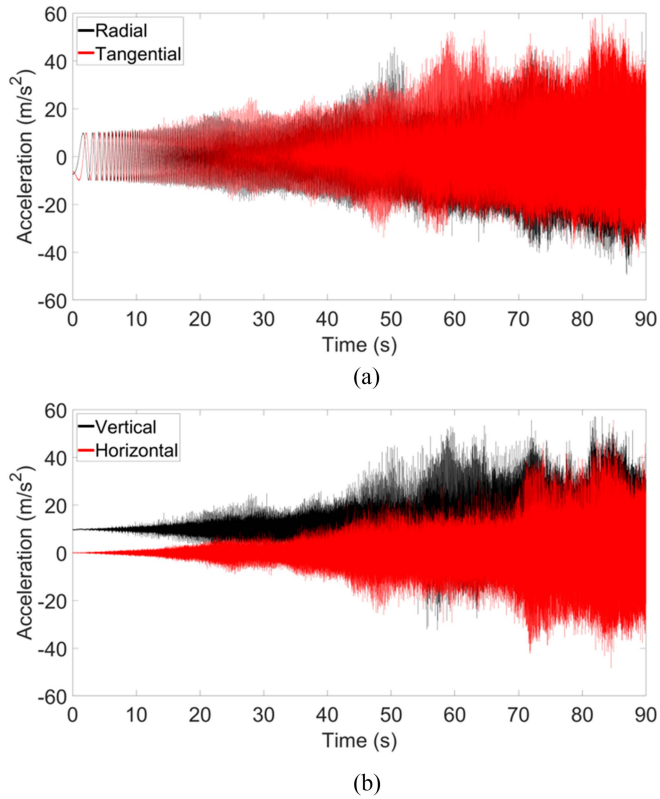

Fig. 6. Lateral vibration measured with the UMU. (a) Lateral vibration calculated from tangential acceleration data and radial acceleration data. (b) Vertical and horizontal lateral vibration calculated from data presented in (a).

3) Calculate the vertical and horizontal vibration with the rotation matrix (22). The results from (17), (19), and (21) are substituted to

$$\begin{bmatrix} a_{lvm}(n) \\ a_{lhm}(n) \end{bmatrix} = \begin{bmatrix} \cos(\beta(n)) & -\sin(\beta(n)) \\ \sin(\beta(n)) & \cos(\beta(n)) \end{bmatrix} \cdot \begin{bmatrix} a_{lt}(n) \\ a_{lr}(n) \end{bmatrix} \tag{22}$$

where n is the sample number, a_{lvm} is the vertical lateral vibration calculated with the rotation matrix, and a_{lhm} is the horizontal lateral vibration calculated with the rotation matrix.

By substituting (18) and (20) to (22), (22) will yield the following result:

$$\begin{bmatrix} a_{lvm}(n) \\ a_{lhm}(n) \end{bmatrix} = \begin{bmatrix} g - a_{lv} \\ a_{lh} \end{bmatrix}. \tag{23}$$

The result shows that the horizontal vibration vector does not include the gravitational component anymore, but the vertical vibration still does. However, the gravitational component is only a constant at this point, which can be removed leaving only the vertical vibration. Now the torsional, vertical lateral, and horizontal lateral vibration are separated from each other as well as the gravitational component removed.

3) Velocity: Velocity in rounds per minute can be calculated from the radial acceleration data with the following equation:

$$\omega_{\mathrm{r/min}} = \sqrt{\frac{|a_{tr}|}{r}} \cdot \left(\frac{60}{2\pi}\right) \tag{24}$$

where a_{tr} is the radial torsional acceleration and r is the distance of the sensor from the shaft central axis. The absolute value of the radial acceleration is inserted to the square root to eliminate imaginary results if the acceleration is temporarily negative. Small miss alignment of the sensors can cause the calculated radial torsional acceleration to get negative values when velocity is low.

4) Frequency Domain Data Analysis: In condition monitoring, the frequency and the amplitude of the vibration signals are typically the interesting components from the perspective of machine operation and condition. A DFT is a good method to use when the signal is periodic, i.e., the machine is running with a constant speed and there are no sudden changes in the excitations of the system. However, this is not always the case, e.g., with a ship powertrain, the motor/propeller velocity changes depending on the velocity the ship is operated and that can make the signal nonperiodic. For this purpose, several different time-frequency analyses (TFA) have been developed [17]. In this article, the measurements were conducted during powertrain acceleration (see Section II-D); hence, TFA is required to observe how the vibration changes over time. A short time Fourier analysis (STFT) is selected to perform TFA. STFT divides the time domain signal into segments and performs a fast Fourier transform (FFT) for each of the segments separately. The segmented frequency domain signals are plotted in a three-dimensional (3-D) plot where the axes are time, amplitude, and frequency. Typically, the segments are windowed before applying FFT, as was done with a Hanning window to the data presented in this research. Of noteworthy interest, STFT has also been applied in other condition monitoring-related publications [11], [18], [19].

To enable more accurate comparison of reference sensors and UMU, the measurement signals were time synced. First, the data of the UMU was resampled to match with the data of the reference sensors. Second, cross correlation was used to define the number of samples that were required to shift the original reference signal. The plots presented, in this article, were done with the original UMU data and shifted reference sensors data.

D. Test Setup and Measurements

The tests were conducted with a small-scale maritime powertrain test bench presented in Fig. 3. The test bench is designed for research related to digital twins, predictive maintenance, and virtual, wireless, and wired sensors. The test bench consisted of two servomotors. One worked as a driving motor, and the other one as a torsional excitation and load source. The test bench also had a lateral sinusoidal excitation device (component 3 in Figs. 3 and 4), which consisted of a 24-volt small dc motor and an unbalance in the motor shaft. The dc motor could be rotated with different velocities, and the unbalance causes lateral vibration at the rotational speed. The test bench had three planetary gears, with gear ratios of 1:3, 1:4, and 8:1. The 1:3 and 1:4 gears

TABLE III
SPECIFICATIONS OF HS-1005005001 (HANSFORD SENSORS) AND DRBK-20 (ETH MESSTECHNIK)

	HS-100	DRBK-20
Measurement range	±16 g	±20 Nm
Sensitivity	500 mV/g	4 V/Nm
Bandwidth	10 kHz	1 kHz

are the angle gears visible in the Fig. 3(marked with 4 and 5), and the 8:1 gear is the gear before the load motor. The two lowest visible torsional natural frequencies of the system are approximately 29 Hz and 66 Hz. These are determined with a simulation model in MATLAB using Simscape, experimental studies, and an open-source tool for torsional vibration analysis called openTorsion.

The UMU, reference sensors, and lateral sinusoidal excitation device are presented in Fig. 4. To compare and verify the results of the UMU, several reference sensors were used: two one-axis integrated electronics piezo-electric (IEPE) accelerometers (HS-1005005001), an optical incremental encoder with 5000 pulses per revolution (ERN 420), and a torque transducer (DRBK-20). Specifications of the reference accelerometer and torque transducer can be found in Table III. The reference accelerometers were mounted to the bearing housing to measure the lateral vibration, and the encoder and torque transducer were mounted to the shaft. The encoder was utilized to measure the velocity, and the torque transducer measured the torsional vibration. The data acquisition of the reference sensors was realized with National Instrument's cRIO-9057 and measurement modules NI-9215, NI-9411, and NI-9234. The lateral sinusoidal excitation device was controlled with a laboratory power source to provide accurate control voltage.

The test measurement was done with a constant acceleration from 0 to 1500 r/min in 90 s. The load motor was set to produce a constant torsional sinusoidal torque excitation at 15, 43, and 87 Hz, and the lateral excitation device was set to produce a constant sinusoidal lateral excitation at around 21 Hz. The reference sensors utilized a sampling rate of 3 kHz, and UMU was sampling at 10 kHz. The UMU was configured to use a ±40 g measurement range during the tests.

III. RESULTS

The results were produced as explained in chapter II. The UMU data are compared to the reference sensors in the following ways: torsional vibration is compared to the torque transducer; lateral vibration is compared to the accelerometers mounted to the bearing housing; and the angle and velocity are compared to hall sensor on the UMU and to the optical encoder mounted to the shaft.

A. Torsional and Lateral Vibration

The raw measurement data from the UMU was processed with the procedure presented in Section II. The data processing method is presented using STFT plots in Fig. 5. The topmost plot (a) presents the raw acceleration data, which are divided into lateral [plot (b)] and torsional vibration [plot (c)], and the lateral vibration is further divided into vertical [plot (d)] and horizontal vibration [plot (e)]. Before the lateral vibration is divided into vertical and horizontal vibration, V-shape lines are visible in the plot. These start at 21, 43, and 87 Hz, which are the frequencies at which the load motor and the lateral excitation device excite the system. This phenomenon is caused by amplitude modulation. Because the sensors are rotating with the shaft, the lateral vibration changes direction in the coordinate system of the sensors as a function of the rotation frequency. The distance of the V-shape lines is equal to two times the rotating frequency, and the mean value of the two lines provide the correct frequency for the lateral excitation. The plots (d) and (e) show that the coordinate transformation matrix (22) for separating the vertical and horizontal lateral vibration from lateral vibration data demodulates the amplitude modulation as well and gives one excitation peak per excitation.

Fig. 6 presents the time domain data of the Fig. 5 plots (d) and (e) as well as the lateral vibration calculated with (17) and (19). The plot (b) of Fig. 6 shows that after the coordinate transformation the vertical vibration has a constant offset of around 9.8 m/s^2 and vertical close to 0 m/s^2, and the gravitational sinusoidal component from the rotation of the sensor is removed.

Fig. 7 presents the lateral vibration of the system. Plots (a) and (b) present the vertical lateral vibration, and plots (c) and (d) present the horizontal lateral vibration measured with the UMU and reference accelerometers. The plots show clear peaks at 21, 43, and 87 Hz (red dashed lines) throughout the whole acceleration, but the lowest torsional excitation produced by the load motor (15 Hz) is not that distinct except in the vertical reference accelerometer [plot (b)]. In addition, the horizontal plots present vibration in around 66 Hz. This is a second lowest visible torsional natural frequency, which is also visible in the torsional vibration plot in Fig. 8. The velocity of the shaft in rounds per second (RPS) is marked with white dashed line. The horizontal reference accelerometer shows a lateral natural frequency of the system at 8.5 Hz. However, this is not visible in the data of the UMU. The low frequencies (below ∼15 Hz) are not as clear in the UMU data than on the reference accelerometers data. Nevertheless, with the higher frequencies, the results are more similar.

Fig. 8 presents the STFT of the torsional vibration calculated from the UMU data with (13) and torsional vibration measured with the torque transducer. Both plots are similar, and the same information is visible. The torsional excitations produced by the load motor (15, 43, and 87 Hz) are clearly visible in the plots. The two lowest visible torsional natural frequencies are also presented in both plots. The natural frequencies occur at 29 Hz and 66 Hz. In addition, the rotation velocity as RPS is highlighted in the plots with a white dashed line.

Figs. 9 and Fig. 10 present single time segments from the time STFT plots to enable better comparison quantitatively between the UMU and reference sensors. In addition, Tables IV–VI presents numerical values from the Figs. 7 and Fig. 8, which further enables comparison of the UMU and reference sensors. The tables and Figs show that the frequencies are similar, but the amplitudes have differences. The amplitude differences can have several reasons, which are discussed in Section IV-A.

TABLE IV
AMPLITUDES AND FREQUENCIES OF VERTICAL LATERAL EXCITATIONS MARKED IN FIG. 7(PLOTS A AND B)

Time	UMU						Reference accelerometer					
	Lateral excitation (21 Hz)		Second torsional excitation (43 Hz)		Third torsional excitation (87 Hz)		Lateral excitation (21 Hz)		Second torsional excitation (43 Hz)		Third torsional excitation (87 Hz)	
(s)	A (m/s^2)	f (Hz)	A (m/s^2)	f (Hz)	A (m/s^2)	f (Hz)	A (m/s^2)	f (Hz)	A (m/s^2)	f (Hz)	A (m/s^2)	f (Hz)
20	0.0332	21.2505	0.0331	43.0011	0.0282	87.0022	0.0337	21.2519	0.0450	43.0038	0.0207	87.0076
40	0.0407	21.0005	0.0403	43.0011	0.0192	87.0022	0.0355	21.0018	0.0414	43.0038	0.0142	87.0076
60	0.0369	20.7505	0.0413	43.0011	0.0184	87.0022	0.0330	20.7518	0.0385	43.0038	0.0199	87.0076
80	0.0353	20.5005	0.0473	43.0011	0.0454	87.0022	0.0331	20.5018	0.0395	43.0038	0.0339	87.0076

TABLE V
AMPLITUDES AND FREQUENCIES OF HORIZONTAL LATERAL EXCITATIONS MARKED IN FIG. 7 (PLOTS C AND D)

Time	UMU						Reference accelerometer					
	Lateral excitation (21 Hz)		Second torsional excitation (43 Hz)		Third torsional excitation (87 Hz)		Lateral excitation (21 Hz)		Second torsional excitation (43 Hz)		Third torsional excitation (87 Hz)	
(s)	A (m/s^2)	f (Hz)	A (m/s^2)	f (Hz)	A (m/s^2)	f (Hz)	A (m/s^2)	f (Hz)	A (m/s^2)	f (Hz)	A (m/s^2)	f (Hz)
20	0.0050	21.2505	0.0046	43.0011	0.0054	87.0022	0.0030	21.2519	0.0052	43.0038	0.0087	87.0076
40	0.0107	21.0005	0.0099	43.0011	0.0101	87.0022	0.0032	21.0018	0.0036	43.0038	0.0117	87.0076
60	0.0142	20.7505	0.0123	43.0011	0.0109	87.0022	0.0029	20.7518	0.0036	43.0038	0.0102	87.0076
80	0.0226	20.5005	0.0289	43.0011	0.0466	87.0022	0.0031	20.5018	0.0052	43.0038	0.0099	87.0076

TABLE VI
AMPLITUDES AND FREQUENCIES OF THE PRODUCED TORSIONAL EXCITATIONS MARKED IN FIG. 8

Time	UMU						Reference torque transducer					
	First torsional excitation (15 Hz)		Second torsional excitation (43 Hz)		Third torsional excitation (87 Hz)		First torsional excitation (15 Hz)		Second torsional excitation (43 Hz)		Third torsional excitation (87 Hz)	
(s)	A (m/s^2)	f (Hz)	A (m/s^2)	f (Hz)	A (m/s^2)	f (Hz)	A (Nm)	f (Hz)	A (Nm)	f (Hz)	A (Nm)	f (Hz)
20	0.0771	15.0004	0.2304	43.0011	0.2191	87.0022	0.0547	15.0013	0.0485	43.0038	0.0072	87.0076
40	0.0633	15.0004	0.2233	43.0011	0.1783	87.0022	0.0456	15.0013	0.0454	43.0038	0.0053	87.0076
60	0.0682	15.0004	0.2104	43.0011	0.1832	87.0022	0.0518	15.0013	0.0423	43.0038	0.0056	87.0076
80	0.0439	15.0004	0.2192	43.0011	0.1752	87.0022	0.0514	15.0013	0.0446	43.0038	0.0067	87.0076

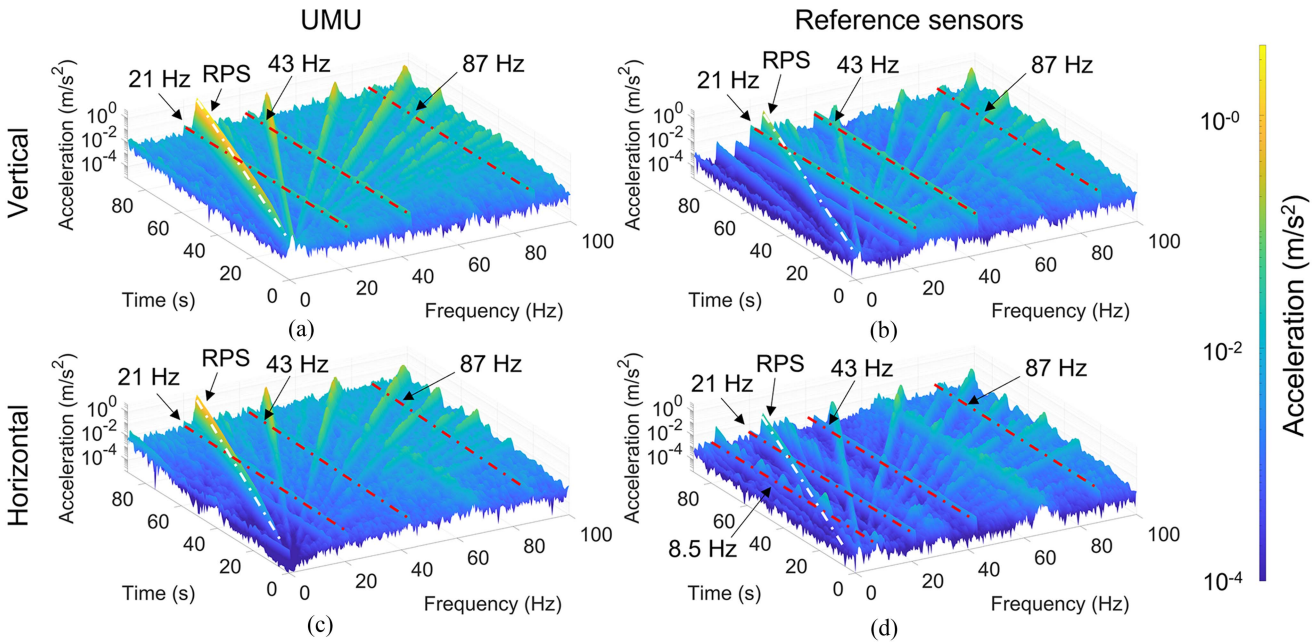

Fig. 7. STFT of lateral vibration measured with the UMU [plots (a) and (c)] and reference accelerometers on bearing housing [plots (b) and (d)]. Plots (a) and (b) present the vertical lateral vibration, and plots (c) and (d) present the horizontal lateral vibration. The white dashed line is the velocity (RPS). The red dashed lines present the constant excitations in the system. 21 Hz is produced by the sinusoidal lateral excitation device, and 43 and 87 Hz are the torsional vibration produced by the load motor. Plot (d) also presents the frequency around 8.5 Hz, which is the horizontal lateral natural frequency of the system. *Y*-axis has a logarithmic scale.

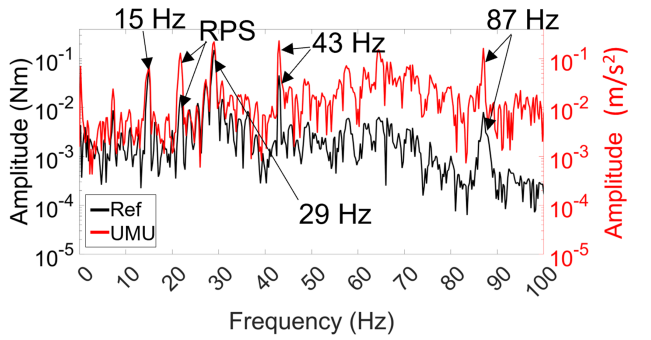

Fig. 8. Single time segments from lateral vibration presented in Fig. 7 at around 88 s. (a) Presents single time segments of vertical lateral vibration. (b) Horizontal lateral vibration. RPS marks the revolutions per second and ref is the reference sensor. *Y*-axis has a logarithmic scale.

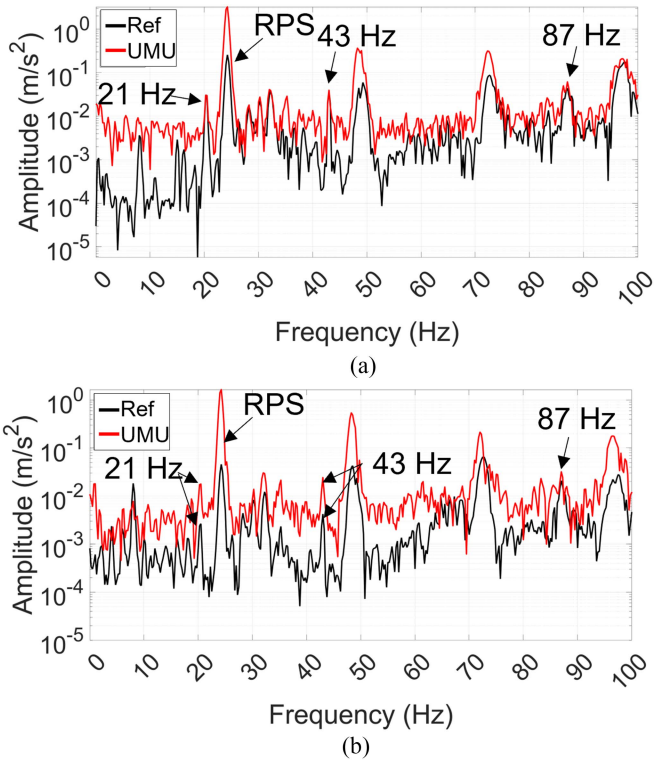

Fig. 9. STFT of torsional vibration measured with the UMU [plot (a)] and reference torque transducer [plot (b)]. The white dashed line is the velocity (RPS). The red dashed lines present the 15, 43, and 87 Hz frequencies that the load motor produces, and 29 Hz and 65.5 Hz are the two lowest natural frequencies visible in the system. *Y*-axis has a logarithmic scale.

B. Velocity and Angle

The velocity calculated from the acceleration data is compared to the velocity from the reference encoder in Fig. 11(a). In low velocities, below 50 r/min, the velocity based on acceleration struggles but with higher velocities, it is comparable to the encoder velocity. From the angle difference between each hall sensor pulse calculated from the acceleration data [see Fig. 11(b)], the opposite can be observed. In lower velocities, the accuracy is better and with higher velocities the fluctuation of the angle value is greater. The angle value between the pulses stays within the range of 362.2 and 357.9 degrees during the acceleration.

IV. Discussion

The results show that the UMU with the presented signal processing method can measure torsional and lateral vibration directly from the shaft. The frequencies were measured accurately but the amplitudes could not be compared adequately to the reference sensors because they were measuring either different components of the machine or different physical phenomena. The presented signal processing method also enables separate inspection of the horizontal and vertical lateral vibration. The lateral vibration measurements show some of the same frequencies as the torsional vibration measurements. They show the torsional vibration occurring at 43 and 87 Hz and the horizontal lateral vibration data show the second lowest visible torsional natural frequency at circa 66 Hz. This is due to a coupling effect caused by for example an unbalance [20], [21] or the gears [22]. It is not studied what exactly causes the coupling effect in the test bench, but the reference measurements present the same phenomena as the measurements of the UMU, which is enough for the validation of the UMU.

A. Vibration Measurement Uncertainty

The reference sensors and the UMU detected similar vibration in the lateral directions, which was over 20 Hz. However, the low frequency lateral vibration was harder to detect with the UMU compared to the reference sensors. In addition, the amplitudes have some differences. These can be caused by several factors as follows:

1) The UMU and reference sensors are mounted to different parts of the powertrain.
2) The MEMS accelerometers have a typically higher noise floor than IEPE accelerometers.
3) There can be a small misalignment with the MEMS accelerometers in the UMU.

Vibration might occur differently in different components of a powertrain, which can make two sensors to measure different vibration from the same powertrain. This might be one of the reasons why the low frequencies appeared differently when comparing the data from the UMU and reference accelerometers. In addition, the measurement of different components could affect the amplitude both sensors measured. However, this would need more research to know more accurately how much the mounting location affects the measured vibration. The higher noise floor of the MEMS accelerometers can be detected from Figs. 7 and 9. This is especially visible in the low frequencies, which makes the low amplitude vibration harder to detect with the UMU. The third contributing factor might be a small misalignment with the UMU accelerometers. The alignment is crucial to the measurement because misalignment will change the sensor measurement angles and will affect the signal processing accuracy.

The torsional vibration was measured sufficiently with the UMU. They presented the similar frequencies for the vibration, but the amplitudes have differences. The most likely reason for the different amplitudes is that the sensors were measuring

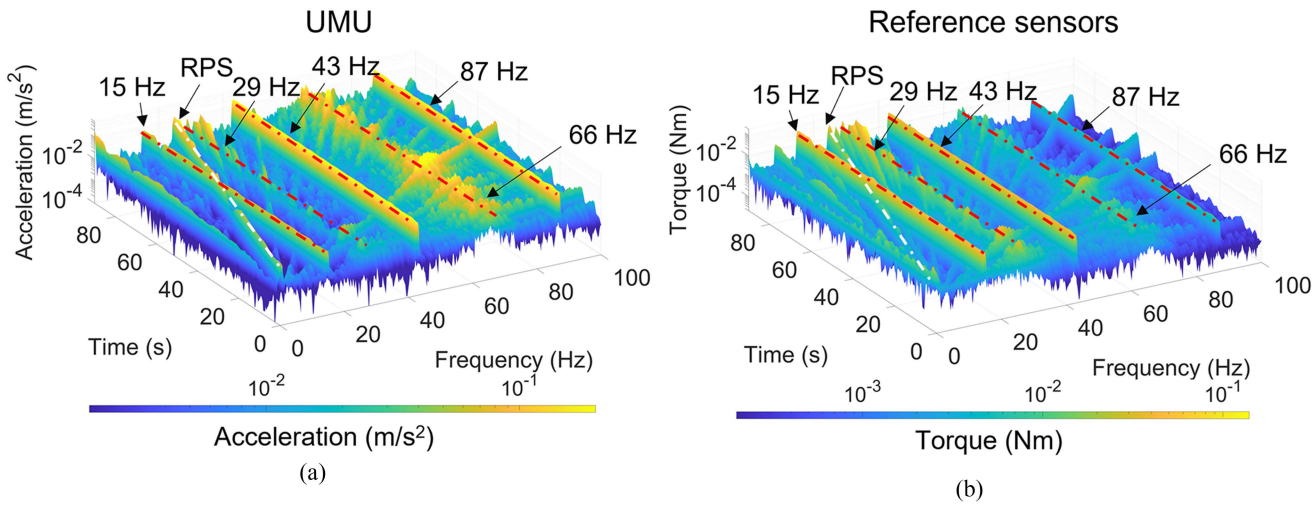

Fig. 10. Single time segments from torsional vibration presented in Fig. 8 at around 80 s. RPS marks the revolutions per second and ref is the reference sensor. *Y*-axis has a logarithmic scale.

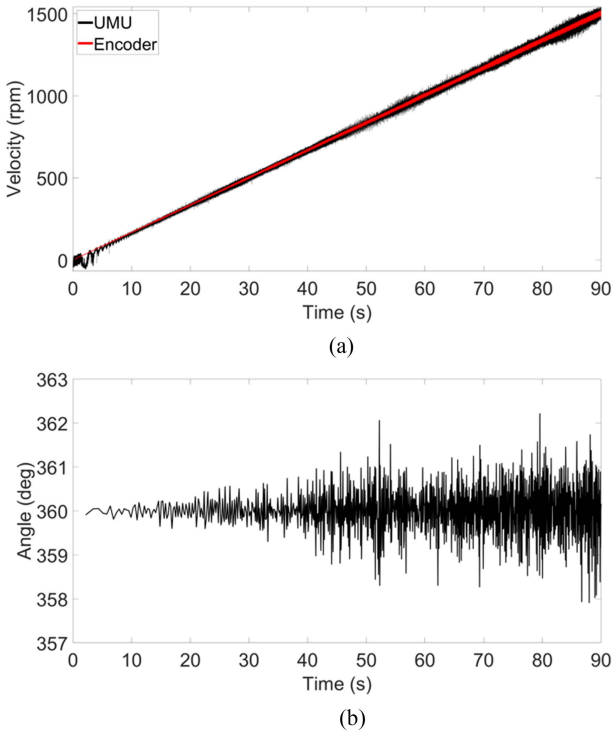

Fig. 11. (a) Velocity calculated from the UMU radial acceleration data compared to the encoder velocity. (b) Angle difference between hall sensor pulses calculated from the UMU acceleration data.

different physical phenomena from the machine; the UMU was measuring tangential acceleration when the reference torque transducer was measuring deformation (twist) of the shaft. The signal processing separated the torsional vibration well from the raw acceleration data, and no significant lateral vibration is visible in the torsional vibration data. The same torsional vibrations are visible in the data of the UMU as well as in the data of the reference sensor. Neither of them detects the vibrations caused by the sinusoidal lateral excitation device at 21 Hz.

B. Benefits of the UMU

The UMU provides an advantage compared to the reference sensors in several ways: it is wireless, easy to mount, and cost-effective, and one measurement instrument can replace several different sensors. By adding the presented signal processing method to the equation, one of the major advantages, which arises is that with a single device, the lateral, and torsional vibration can be measured and separated with a high degree of accuracy.

The UMU could be used for fault diagnosis of rotating machinery. Typically, for example accelerometers mounted to the gearbox are utilized to gather data from machines, and traditional signal processing or the increasingly popular machine learning techniques are used to identify the fault type [23]–[27]. The UMU could provide more information for fault diagnostic algorithms, with simpler measurement installation compared to the commonly used accelerometer setups. In addition, the UMU could do some pre calculations for the data before it is sent to the user in the spirit of edge computing.

Some of the torsional vibrations are visible in the lateral vibration due to the coupling effect. The UMU could enable identification, which vibrations are originated from torsional and which from lateral vibration without complex and expensive measurement setup.

C. Accuracy of Velocity and Angle

The UMU can also measure velocity and angle. The results show similar velocities when compared to the reference encoder with higher velocities. However, with low velocities, below 50 r/min, some fluctuation can be observed. A possible reason to explain this is that the accelerometers of the UMU are not perfectly aligned, which leaves some sinusoidal component from the gravity to the calculated radial torsional acceleration data. This residual sinusoidal component is large compared to the other accelerations in the system at low velocities, which causes this fluctuation. When the velocity increases, the constant radial

acceleration increases as well, but the small residual sinusoidal component remains constant. Hence, the fluctuation caused by the residual component decreases.

The angle calculated from the acceleration data between each hall sensor pulse is presented in Fig. 11(b). This should give a constant value of 360°, but there is some variation between 362.2 and 357.9° and the variation is larger with higher velocities. The angle was calculated with the gravitation component of the tangential and radial lateral vibration. However, when the shaft rotates with higher velocities, there are more vibration accruing close to the rotating frequency (i.e., the frequency of the gravitational component), which causes this variation. In addition, misalignment of the accelerometers can influence the angle accuracy.

D. Constant Radial Acceleration and Larger Shaft

When accelerometer is mounted to a rotating shaft, it is under a constant radial acceleration, which causes stress to the sensing elements. However, during this study, an assumption has been made that if the affecting acceleration does not exceed the measurement range of the sensor, it should not affect the measurement. The maximum acceleration during the tests was circa 230 m/s^2, which is approximately half of the full measurement range. The results also indicate that the assumption can be made, because similar measured phenomena as the UMU measures, can be observed from the reference sensors as well.

The tests were conducted with a small-scale maritime powertrain test bench, which had a shaft diameter of 8 mm. With larger shaft diameters yet same rotating frequencies, a different accelerometer with wider measurement range may be needed.

V. Conclusion

This article presented a wireless UMU with innovative combination of features for lateral and torsional vibration measurement directly from the rotating shaft using two MEMS accelerometers mounted to the opposite sides of the shaft. The data are processed with a novel signal processing method, which deletes the gravitational acceleration and separates the torsional and lateral vibration from each other, in addition to decomposing the lateral vibration in horizontal and vertical directions. The UMU and presented signal processing method was tested in a small-scale maritime powertrain test setup and compared to reference sensors. The results indicate that the UMU and signal processing method worked well. The presented method separated and detected the torsional and lateral vibration with sufficient accuracy. Nevertheless, more research needs to be conducted on the alignment of the accelerometers. As alignment problems can affect the accuracy of the measurement, the degree of permitted misalignment needs to be studied in the future.

References

[1] D. Remond, "Practical performances of high-speed measurement of gear transmission error or torsional vibrations with optical encoders," *Meas. Sci. Technol.*, vol. 9, no. 3, pp. 347–353, 1998, doi: 10.1088/0957-0233/9/3/006.

[2] H. Luo, R. Chumai, N. Peton, B. Howard, and A. Menon, "Torsional vibration detection using high sampling rate and high resolution keyphasor information," in *Proc. ASME Des. Eng. Tech. Conf.*, 2013, vol. 8, pp. 1–12, doi: 10.1115/DETC2013-12367.

[3] F. C. Gómez De León and P. A. Merõo Pérez, "Discrete time interval measurement system: Fundamentals, resolution and errors in the measurement of angular vibrations," *Meas. Sci. Technol.*, vol. 21, no. 7, 2010, Art. no. 075101, doi: 10.1088/0957-0233/21/7/075101.

[4] M. Hilal Muftah, M. Mohamed Haris, K. Petroczki, and E. Awad Khidir, "An improved strain gauge-based dynamic torque measurement method," *Int. J. Circuits, Syst. Signal Process.*, vol. 7, no. 1, pp. 66–73, 2013.

[5] K. Hoffmann, "Applying the wheatstone bridge circuit," *Nucl. Instruments Methods*, vol. 150, no. 3, pp. 597–598, 1978, doi: 10.1016/0029-554X(78)90136-2.

[6] S. Ahn et al., "Development of micro torque measurement device using strain gauge," in *Proc. IEEE Int. Symp. Assem. Manuf.*, 2009, pp. 101–106.

[7] S. Lin and J.-H. Kuang, "Accelerometer pair measurements for shaft dynamic parameters analysis," in *Proc. SPIE- Int. Soc. Opt. Eng.*, 1994, pp. 1649–1655.

[8] Z. Mones, G. Feng, X. Tang, U. Haba, F. Gu, and A. D. Ball, "A comparative study of gravitational acceleration cancellation from on-rotor MEMS accelerometers for condition monitoring," in *Proc. 24th Int. Congr. Sound Vib.*, 2017, pp. 1–8.

[9] M. Elnady, "On-Shaft vibration measurement using a MEMS accelerometer for faults diagnosis in rotating machines," Ph.D. dissertation, Univ. of Manchester, Manchester, U.K., 2013.

[10] I. Koene, R. Viitala, and P. Kuosmanen, "Vibration monitoring of a large rotor utilizing internet of things based on-shaft MEMS accelerometer with inverse encoder," in *Proc. 12th Int. Conf. Rotating Mach.*, 2020, pp. 498–510.

[11] M. E. Elnady, J. K. Sinha, and S. O. Oyadiji, "Identification of critical speeds of rotating machines using on-shaft wireless vibration measurement," *J. Phys., Conf. Ser.*, vol. 364, 2012, Art. no. 012142, doi: 10.1088/1742-6596/364/1/012142.

[12] L. Baghli, J. F. Pautex, and S. Mezani, "Wireless instantaneous torque measurement, application to induction motors," in *Proc. 19th Int. Conf. Elect. Mach.*, 2010, pp. 1–6, doi: 10.1109/ICELMACH.2010.5608217.

[13] S. Jiménez, M. O. T. Cole, and P. S. Keogh, "Vibration sensing in smart machine rotors using internal MEMS accelerometers," *J. Sound Vib.*, vol. 377, pp. 58–75, Sep. 2016, doi: 10.1016/j.jsv.2016.05.014.

[14] M. Martinez, D. Fernandez, D. Reigosa, J. M. Guerrero, and F. Briz, "Wireless torque pulsations measurement system for PMSMs," *IEEE Trans. Ind. Appl.*, vol. 56, no. 6, pp. 6467–6476, Nov./Dec. 2020, doi: 10.1109/TIA.2020.3012956.

[15] G. Feng, N. Hu, Z. Mones, F. Gu, and A. D. Ball, "An investigation of the orthogonal outputs from an on-rotor MEMS accelerometer for reciprocating compressor condition monitoring," *Mech. Syst. Signal Process.*, vol. 76/77, pp. 228–241, 2016, doi: 10.1016/j.ymssp.2015.12.033.

[16] I. Koene, V. Klar, and R. Viitala, "IoT connected device for vibration analysis and measurement," *HardwareX*, vol. 7, Apr. 2020, Art. no. e00109, doi: 10.1016/j.ohx.2020.e00109.

[17] E. Sejdić, I. Djurović, and J. Jiang, "Time-frequency feature representation using energy concentration: An overview of recent advances," *Digit. Signal Process., A Rev. J.*, vol. 19, no. 1, pp. 153–183, 2009, doi: 10.1016/j.dsp.2007.12.004.

[18] I. Koene, R. Viitala, and P. Kuosmanen, "Vibration analysis of a large rotor over industrial internet," in *Proc. 59th Ilmenau Sci. Colloq.*, 2017, pp. 1–9.

[19] I. Koene, R. Viitala, and P. Kuosmanen, "Internet of things based monitoring of large rotor vibration with a microelectromechanical systems accelerometer," *IEEE Access*, vol. 7, pp. 92210–92219, 2019, doi: 10.1109/ACCESS.2019.2927793.

[20] B. O. Al-Bedoor, "Modeling the coupled torsional and lateral vibrations of unbalanced rotors," *Comput. Methods Appl. Mech. Eng.*, vol. 190, no. 45, pp. 5999–6008, 2001, doi: 10.1016/S0045-7825(01)00209-2.

[21] A. N. Halilbeşe, C. Zhang, and O. A. Özsoysal, "Effect of coupled torsional and transverse vibrations of the marine propulsion shaft system," *J. Mar. Sci. Appl.*, vol. 20, no. 2, pp. 201–212, Jun. 2021, doi: 10.1007/s11804-021-00205-2.

[22] M. A. Rao, J. Srinivas, V. B. V. Rama Raju, and K. V. S. S. Kumar, "Coupled torsional-lateral vibration analysis of geared shaft systems using mode synthesis," *J. Sound Vib.*, vol. 261, no. 2, pp. 359–364, 2003, doi: 10.1016/S0022-460X(02)01240-3.

[23] J. Li, R. Huang, G. He, Y. Liao, Z. Wang, and W. Li, "A two-stage transfer adversarial network for intelligent fault diagnosis of rotating machinery with multiple new faults," *IEEE/ASME Trans. Mechatronics*, vol. 4435, no. 3, pp. 1591–1601, Jun. 2021, doi: 10.1109/tmech.2020.3025615.

[24] H. Shao, M. Xia, J. Wan, and C. De Silva, "Modified stacked Auto-encoder using adaptive morlet wavelet for intelligent fault diagnosis of rotating machinery," *IEEE/ASME Trans. Mechatronics*, vol. 27, no. 1, pp. 24–33, Feb. 2022, doi: 10.1109/TMECH.2021.3058061.

[25] X. Wang, Z. Yang, and X. Yan, "Novel particle swarm optimization-based variational mode decomposition method for the fault diagnosis of complex rotating machinery," *IEEE/ASME Trans. Mechatronics*, vol. 23, no. 1, pp. 68–79, Feb. 2018, doi: 10.1109/TMECH.2017.2787686.

[26] S. Chen, Y. Meng, H. Tang, Y. Tian, N. He, and C. Shao, "Robust deep learning-based diagnosis of mixed faults in rotating machinery," *IEEE/ASME Trans. Mechatronics*, vol. 25, no. 5, pp. 2167–2176, 2020, doi: 10.1109/TMECH.2020.3007441.

[27] H. Li, J. Huang, X. Yang, J. Luo, L. Zhang, and Y. Pang, "Fault diagnosis for rotating machinery using multiscale permutation entropy and convolutional neural networks," *IEEE/ASME Trans. Mechatronics*, vol. 22, no. 8, pp. 101–110, Jul. 2020, doi: 10.3390/E22080851.

Ivar Koene was born in 1993. He received the M.Sc. and D.Sc. degrees in mechanical engineering from Aalto University, Espoo, Finland, in 2018 and 2022, respectively.

He has done research related to how cost-effective IoT sensors could be utilized in the condition monitoring of large rotating machinery and powertrains. He is also involved in digital twin-related research, where one of the goals is to utilize a digital twin for predictive maintenance.

Sampo Haikonen received the B.Sc. degree in mechanical engineering in 2021 from Aalto University, Espoo, Finland, where he is currently working toward the M.Sc. degree in mechanical engineering.

His research interests include vibration measurements and condition monitoring of rotating machinery.

Tuomas Tiainen received the M.Sc. and D.Sc. degrees in mechanical engineering from Aalto University, Espoo, Finland, in 2018 and 2020, respectively.

In his master's thesis he developed an automatic assessment system for mechanical engineering CAD exercises. He completed his doctoral dissertation on multiprobe roundness measurement of large rotors in late 2020. In 2020, he visited Technische Universität Darmstadt researching magnetic bearings and rotating machinery. His current research interests include geometry measurement of large rotors, rotor dynamics, and machine direction analysis methods in paper and cardboard making.

Mikael Manngård (Graduate Student Member, IEEE) was born in 1988. He received the B.Sc. degree in chemical engineering and the M.Sc. (with distinction) in process and systems engineering both in 2013 from Åbo Akademi University, Turku, Finland, where he is currently working toward the Ph.D. degree in process control with the Faculty of Science and Engineering.

His research interests include virtual sensing, system identification, and digital twin development for maritime systems.

Raine Viitala was born in 1992. He received the M.Sc. and D.Sc. degrees in mechanical engineering from Aalto University, Espoo, Finland, in 2017 and 2018, respectively.

His doctoral dissertation was acknowledged with the Aalto University School of Engineering dissertation award. In 2018, he visited Technische Universität Darmstadt, researching rotating kinetic energy storages, i.e., flywheels. His work can be widely applied in several industrial applications, such as electric motors and generators, turbines, and paper machines. He leads a consortium developing AI methods to measure rotor systems and rotor-governed processes. He is instructing students at all academic levels. In addition, he lectures in a bachelor-level course Mechatronics Basics. His research interests include a solid background in experimental large rotor research, including vibration analysis and subcritical vibrations, bearing excitations, roundness measurements, and manufacturing for operating conditions.

Joni Keski-Rahkonen biography not available at the time of publication.